Hindawi
Advances in Materials Science and Engineering
Volume 2019, Article ID 9210713, 8 pages
https://doi.org/10.1155/2019/9210713

Research Article

Directional Solidification of Sn-Cu_6Sn_5 In Situ Composites

Osvaldo Fornaro [1,2]

[1]*Instituto de Física de Materiales Tandil–IFIMAT (UNCPBA), Centro de Investigaciones en Física e Ingeniería del Centro de la Provincia de Buenos Aires-CIFICEN (UNCPBA, CICPBA, CONICET), Pinto 399, B7000GHG Tandil, Argentina*
[2]*Consejo Nacional de Investigaciones Científicas y Técnicas-CONICET, Godoy Cruz 2290, Buenos Aires, Argentina*

Correspondence should be addressed to Osvaldo Fornaro; ofornaro@exa.unicen.edu.ar

Received 28 November 2018; Revised 8 February 2019; Accepted 21 February 2019; Published 13 March 2019

Academic Editor: Luigi Nicolais

The Sn-Cu system presents an important interest from academic and technological point of view because it is part of the family of alloys proposed as lead-free solder alloys for electronic components and also due to the mechanisms involved during the growth of the different phases. Sn-Cu system has two intermetallic phases, i.e., ε-Cu_3Sn and η-Cu_6Sn_5, and η can be used as the negative (anode) electrode in Li-ion batteries, alone or as part of $(Co,Ni)_xCu_{6-x}Sn_5$-type composites. Obtaining this η phase from liquid with the appropriate chemical composition is a very difficult task because it has a formation temperature lower than liquidus for such a composition. In this way, the η phase appears as a consequence of a solid-solid transformation from the ε phase However, it is possible to find the η phase as the primary or secondary phase after a eutectic reaction for lower concentrations of Cu. On the other side, the Cu_6Sn_5 phase shows a hexagonal to monoclinic solid-solid transformation around 187°C, which could affect the mechanical system stability when it is used as solder. In this work, directional solidification at different growth velocities of hypereutectic Sn-Cu samples was performed. The resultant microstructure varies with the growth velocity, but it is formed for a fibber-like primary phase Cu_6Sn_5 which is projected towards the liquid phase. Behind this region, these fibbers are rounded by a two-phase Sn-Cu_6Sn_5 structure. In this way, three zones could to be defined in the sample during the directional growth: (i) an entirely solid two-phase region, formed by η rounded by β(Sn) + η eutectic-like structure, (ii) a two-phase solid (η) + liquid, and (iii) the remnant liquid in front of the interface.

1. Introduction

In the electronics industry, the soldering is one of the most important joining processes applied to connect electronic devices and substrates. Due to harmful effects of lead on environment and human health, a set of strict legislation (the so-called WEEE and RoHS directives) on banning the use of lead-free solders (LFS) were developed [1–5] to replace classical eutectic and near-eutectic Sn-Pb solder alloys. In the last two decades, binary and ternary solders such as Sn-Ag, Sn-Cu, Sn-Zn, Sn-Bi, Sn-Au, Sn-In, Sn-Ag-Cu, Sn-Bi-In, Sn-In-Zn, and Sn-Ag-Bi have been investigated and designed [6, 7]. There are several candidates of LFS Sn-based alloys such as Sn-Ag-Cu alloys (SAC alloys), containing Zn, Bi, and In, which have considerably attracted attention especially for automotive, industrial, and electronic applications. As a part of the process of developing new LFS alloys, thermodynamic calculations have been extensively used [8–11] and a number of thermodynamic databases have been developed specifically for this purpose [9, 11–15]. However, it is well known that a purely thermodynamic approach does not provide direct information on general material properties, such as thermophysical and mechanical properties that are the key to the application of new solder alloys. The knowledge of reliable data related to material properties is essential for the interpretation of alloy solidification and numerical modeling methods for the casting and soldering process. There are several initiatives to obtain a complete alloys properties database [6, 16–20].

For these reasons, there exist considerable experimental works focusing on the characterization of SAC alloys [7, 21–23]. The surface and wetting properties of solders are key properties for design of both the new solders and soldering process [23–25]. The Sn-Cu system is characterized

by the presence of two intermetallic compounds [26]. In the range of temperature and composition of interest, the interfacial reaction results in formation of Cu_3Sn (ε) and Cu_6Sn_5 (η) layers, as already have been observed at the interface of different Sn-based solders in contact with the Cu substrate [23, 27, 28]. Cu_6Sn_5 has two structural forms. Below 187°C (460 K), the stable form is known as η', presenting an ordered long-period superlattice (LPS). During the cooling, the time is usually not sufficient to produce the full transformation $\eta \longrightarrow \eta'$, and the high temperature form remains as the metastable phase [29–31]. Reactive wetting results in the formation of intermetallic phases at the interface of a liquid solder/substrate system which results of interest for the joining process [32–34].

To obtain the η (Cu_6Sn_5) phase from the melting process is necessary follow the solidification path from several concentrations of Sn-Cu alloys. According to the equilibrium phase diagram for Sn-Cu [26], the Cu_6Sn_5 phase may appear as primary or secondary depending on the chemical composition of the alloy. For concentrations greater than 7.44 wt.% Cu, the Cu_3Sn phase is the primary phase and then Cu_6Sn_5 could appear through a solid-solid transformation during the cooling [35]. Taking this in mind, there exist a series of previous works which study the directional solidification of Sn-Cu alloys, both for eutectic compositions as for hypo and hypereutectic alloys [36–38].

Accordingly, the aim of this work is to obtain samples with the appropriate composition that contain η as the primary phase, to be directionally grown under different conditions evaluating the relative stability of that phase and the behavior of the microstructure during the growth.

2. Experimental

The alloys used in this study were obtained, starting from 99.99% purity of Sn and Cu elements, melted in a SiC crucible coated internally by ceramic protective coating, and heated in an electric resistance furnace under constant argon gas flow. Once a homogeneous liquid was obtained, the samples were cast in quartz tubes of similar size, where they would subsequently directionally grow.

Directional growth was performed with a Bridgman-like apparatus, as has been previously reported [39–41]. The device consists of two chambers located in a cylindrical symmetry. Upper chamber consists of an alumina core with a heating coil with an electronic temperature control. The lower section is refrigerated by water circulation. This disposition allows us to obtain a fixed thermal gradient in the place where the samples were located to be directionally grown. The pulling system of the samples was based in a stepper motor and a gear box, which permitted a translation velocity in the 0–10 μm/s range. The actual displacement velocity was measured with a linear variable differential transformer (LVDT) and a signal conditioning interface. After acquisition, the data were sent to a personal computer, which drives the motor. This scheme provides a very precise motion, resulting with a precision of ± 0.1 μm/s. The specimens were located in a quartz tube of 10 mm of internal diameter, with a selected length of 105 mm. The quartz tube was sealed in the bottom with a conical geometry and filled with a partial vacuum of Ar after removing the atmospheric air in several opportunities, to avoid oxide formation during the growth and loses of Cu by reaction with oxygen. During the growth, the thermal gradient in front of the interface was taken in a reference sample by using a double-thermocouple type K using similar pull velocity and furnace temperatures that will be used in the different experiences, resulting in $G_L = 2.5 \pm 0.5$ K/mm. The samples were directionally grown at 0.5, 1.0, 2.0, and 5.0 μm/s and quenched after the solid phase taken approximately 40 mm long.

The preparation of the surface for optical microstructural observation and analysis requires particular attention because this alloy can show plastic deformation during the mechanical polishing giving place to twinning formation and the reprecipitation of small grains on the surface. To avoid these effects, an extremely slow and continuously refrigerated mechanical polishing was made. The microstructure was observed both in longitudinal (respect to the growth direction) and cross-sectional views. The surface was set up by mechanical polishing using alumina grinding papers, up to 0000 grit, and water lubricated. Final mechanical polishing was achieved using micropolish with 2 up to 0.5 μm of Al_2O_3 in water solution. Finally, the samples were electropolished with 2-butoxyethanol (80 ml) + glycerine (10 ml) + $HClO_4$ (10 ml), at 20–30 VCC. The electropolishing process produces an epitaxial oxide epitaxial oxide that let us visualize the structure under polarized light. A chemical etching of HCl (2 ml) + HNO_3 (5 ml) + methanol (93 ml) was used to improve the image contrast under bright light conditions [19, 42].

3. Results and Discussion

Directional growths of samples were carried out at different pulling velocities in the range 0.5 to 5 μm/s under a constant thermal gradient $G_L = 2.5$ K/mm. Obtained microstructures can be seen in Figures 1–4.

As can be seen, the crystal growth is not a simple process. The primary solid phase is a Cu_6Sn_5 intermetallic phase, which appears like projected towards the liquid, because it has a higher liquidus temperature than the rest of the solid. The solidification ends when the liquid reaches the eutectic temperature, at a long distance away. If the different thermal conductivities between different solid phases and the liquid phase were not taken into account, at first order, the distance beyond the top of the interface depends on the thermal gradient and growth rate. In this way, at the moment of quenching, the sample is formed by three zones which can be identified by an entirely quenched liquid, a primary phase plus liquid, and an all solid zone.

Particularly, Figure 1 shows longitudinal cut of a sample grown at $V = 0.5$ μm/s. Figure 1 is divided in two micrographs. In Figure 1(a), it can be seen the zone of top wide faceted the η^P phase and the quenched liquid, whilst in Figure 1(b), it is possible to observe that primary η^P is surrounded by a two-phase $\beta + \eta^S$. Also the primary η^P phase seems to be coarsened by the effect of permanence at high temperature during a longer time.

Note the definition of η^P as the primary η (Cu_6Sn_5) phase in terms of the solidification path to differentiate it with

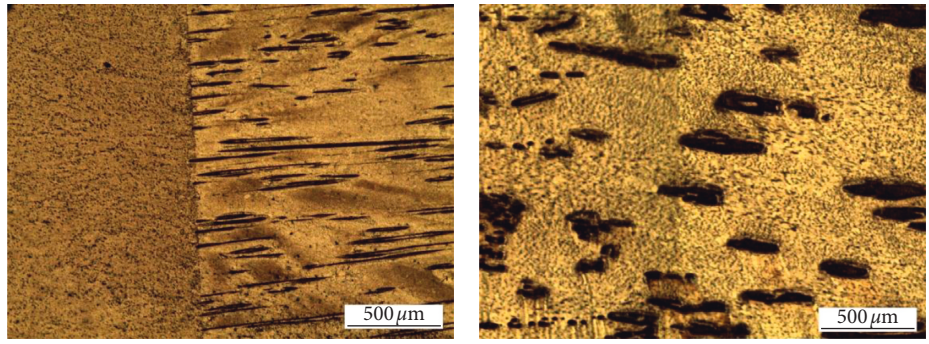

(a) (b)

Figure 1: Sn-0.7 wt.% Cu samples directionally solidified and grown from right to left. $V = 0.5\,\mu$m/s; $G_L = 2.5$ K/mm. Longitudinal view of (a) (η^P + Liq) + Liq. interface at the top of growth; (b) solid + (η^P + Liq) interface.

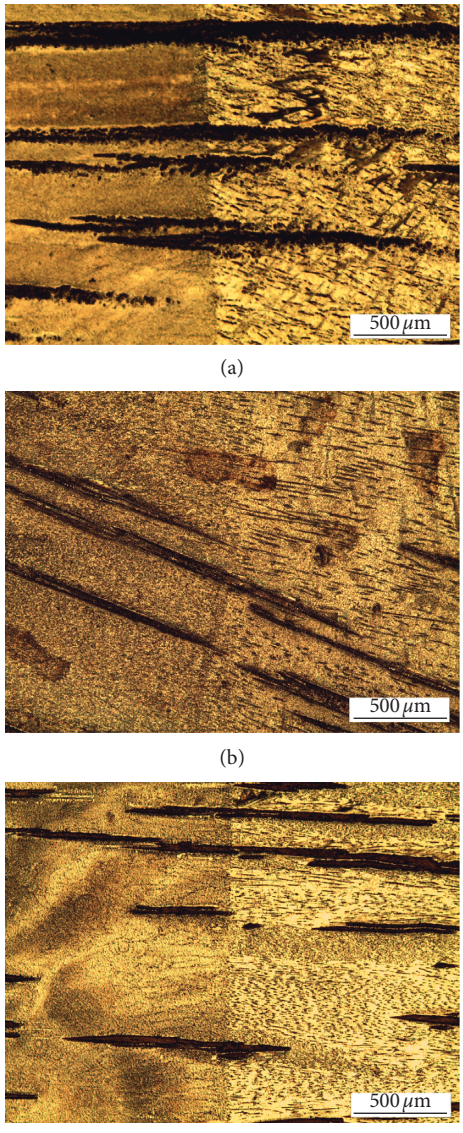

(a)

(b)

(c)

Figure 2: Longitudinal view of Sn-7 wt.% Cu samples directionally grown at increasing values of pulling velocity: (a) 1.0 μm/s; (b) 2.0 μm/s; (c) 5.0 μm/s ($G_L = 2.5$ K/mm).

respect to η^S which appears in the two-phase zone as a consequence of the eutectic reaction of the remaining liquid:

$$\text{liquid} \longrightarrow \beta + \eta^S. \quad (1)$$

Both η^P as η^S have the same composition and structure, but significant difference in size and distribution can be observed in the different micrographs.

Figures 2(a)–2(c) show longitudinal views of samples grown at $V = 1.0$, 2.0, and 5.0 μm/s at the same thermal gradient of $G_L = 2.5$ K/mm. In these micrographs, the zone corresponding to the interface between solid and solid + liquid can be seen. From Figures 2(a)–2(c), the solid is clearly formed by the fibbers of the η phase, surrounded by a two-phase ($\beta + \eta^S$) interfibber zone.

In Figure 3, transverse sections of the growth in the solid zone can be seen. The structure appears similar to the previous figure, showing fibbers of η^P surrounded by an eutectic-like structure ($\beta + \eta^S$). It is clear that η, both as primary and secondary, could transform in the solid state to η' during the cooling of the alloy. Even though micrographs do not appear as evidence of transformation, it is not possible to confirm if this transformation occurs during the growth in some point of the sample. Also from the observation of Figures 1–3, it is evident that a spacing λ_{η^P} and λ_{η^S} could be defined as a function of the solidification growth parameters.

3.1. Phase Fraction Estimation. To interpret the solidification path and the behavior during the growth, it could be useful to use the equilibrium phase diagram of Figure 5. It can be seen that, in the lower Cu content range, this is an eutectic system, with an eutectic composition of $C_E = 0.87$ wt.% Cu and an eutectic temperature $T_E = 226.8$°C (499.95 K). The phases involved into the reaction are β (Sn) and η (Cu_6Sn_5). It can be seen also that both β as η has a limited solubility of the other components (Cu or Sn in each case). Also, η is present in all the range shown, that is from a very dilute alloy up to approximately $C_\varepsilon = 61.63$ wt.% Cu (corresponding to Cu_3Sn composition).

As can be seen from this diagram, different regions could be identified, characterized by the primary phase to nucleate:

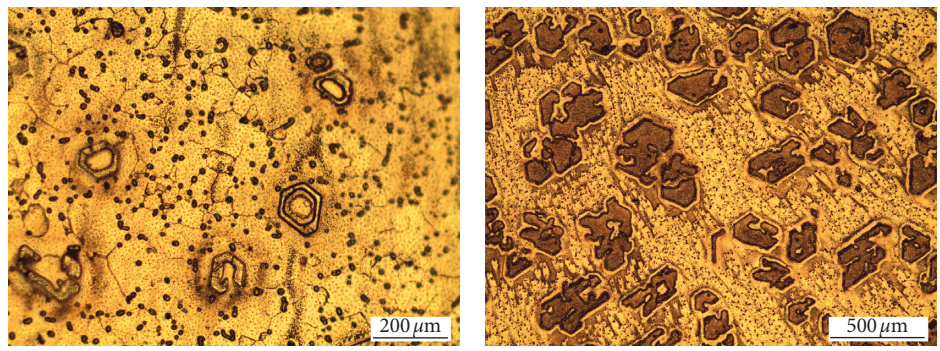

(a) (b)

Figure 3: Transverse sections of samples grown at (a) $V = 0.5\,\mu$m/s and (b) $V = 2.0\,\mu$m/s and $G_L = 2.5$ K/mm.

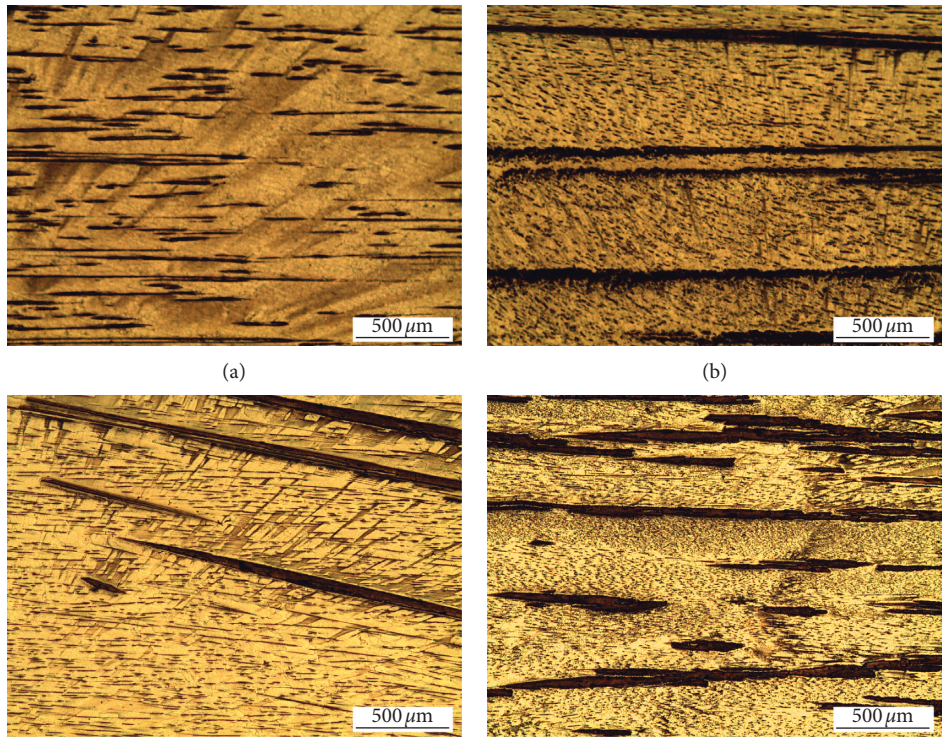

(a) (b)

(c) (d)

Figure 4: Detailed longitudinal views corresponding to the solidified zone (below solid + (η^P + Liq) interface) for different pulling velocities: (a) $V = 0.5\,\mu$m/s; (b) $V = 1.0\,\mu$m/s; (c) $V = 2.0\,\mu$m/s; (d) $V = 5.0\,\mu$m/s. In all cases, $G_L = 2.5$ K/mm.

(i) A dilute alloy or proeutectic zone, for concentrations lesser than 0.87 wt.% Cu. In this case, the primary phase would be β (Sn), and solidification ends with a eutectic reaction like equation (1).

(ii) Hypereutectic alloy, with chemical concentrations greater than 0 87 wt.% Cu but lesser than 7.44 wt.% Cu. In this case, the primary phase is η. The solidification ends with the isothermal eutectic reaction (1).

(iii) Hypereutectic with the chemical composition greater than 7.44 wt.% Cu. The primary phase is the ε (Cu_3Sn) and could transform partially to the η phase, and the final phase fraction depends on the nominal composition of the alloy. In this case, the reaction is formerly a hypoperitectic one:

$$L + \varepsilon \longrightarrow L' + \eta. \tag{2}$$

The situation is condensed in Table 1 and Figure 6, where the phase fraction was calculated at $T \gtrsim T_E$. For this reason, the nominal composition of Sn-7 wt.% Cu was chosen to develop the directional solidification for this work. In this case, and again following equilibrium conditions, the total expected phase fraction of η is small, being close to 20% as a primary phase, f_{η^P}, plus an additional 2% after the eutectic reaction of remnant liquid, f_{η^S}, as can be seen in Figure 7. The solidification path and the present phases for a given

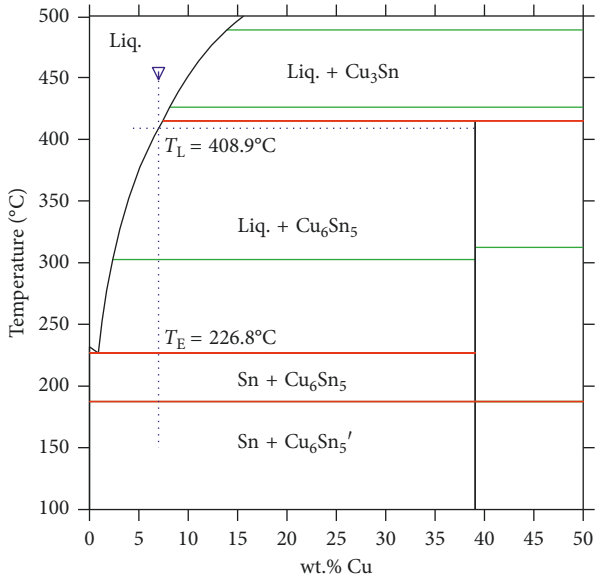

Figure 5: Sn-Cu equilibrium phase diagram.

Table 1: Solidification path of Sn-Cu alloys with different compositions.

Composition range (wt.% Cu)	Primary phase	Secondary phase	Final transformation
0–0.87	β (Sn)	η	$L \longrightarrow \beta + \eta$
0.87	$\beta + \eta$		
0.87–7.44	η	β	$L \longrightarrow \beta + \eta$
7.44–39.07	ε	β	$L + \varepsilon \longrightarrow L' + \beta$ $L' \longrightarrow \beta + \eta$
39.07	ε		$\varepsilon \longrightarrow \eta$
39.07–61.63	ε	η	$L + \varepsilon \longrightarrow \eta$

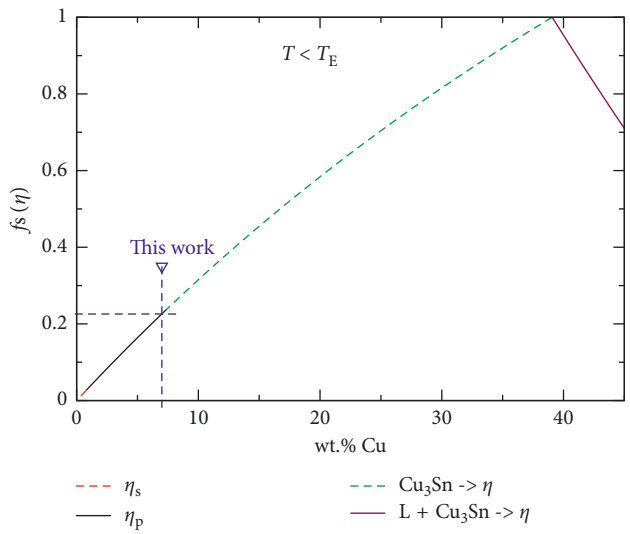

Figure 6: Origin of the η phase depending on the solidification path and composition of the alloy.

value of temperature can be determined under equilibrium considerations by using the lever rule.

The composition of interest for this work is remarked.

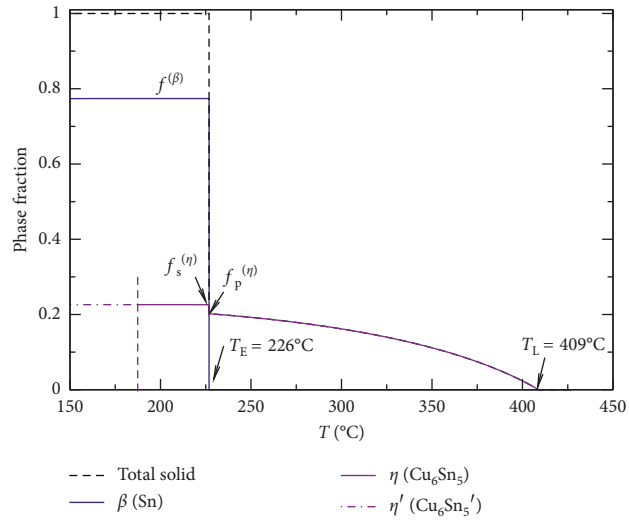

Figure 7: Phase fraction during solidification (calculated under equilibrium considerations).

During the first stage of cooling, the phase fraction of the primary η^{P} in the range between $T_{\mathrm{L}}(C_0)$ and T_{E} could be calculated using

$$f_{\eta^{\mathrm{P}}} = \frac{C_0 - C_{\mathrm{L}}(T)}{C_\eta - C_{\mathrm{L}}(T)}, \tag{3}$$

where C_0 is the nominal composition of the alloy, C_η corresponds to the composition of the η phase, which can be determined from the atomic composition of $\eta = \mathrm{Cu_6Sn_5}$, which results in $C_\eta = 39.1$ wt.% Cu. $C_{\mathrm{L}}(T)$ must be taken from the liquidus line $T_{\mathrm{L}}(C)$ of the phase diagram. Once the system reaches T_{E}, the final reaction (1) implies the isothermal formation of β and η^{S} phases simultaneously. The total η phase fraction is represented in this graph corresponding to the combination of both species ($\eta^{\mathrm{P}} + \eta^{\mathrm{S}}$). In the grown samples, it is possible to observe both values, due to the limited solid diffusion at low temperatures.

3.2. η^P and η^S Spacing. As mentioned above, the limited diffusion of β and η phases results in a wide coupled eutectic zone. In this way, the Jackson–Hunt eutectic theory could be used as a starting point to interpret the obtained microstructures [43, 44]. In principle, this theory is useful for regular nonfaceted/nonfaceted eutectics, which is not this case. However, it can be useful interpret to the behavior of faceted/nonfaceted eutectics, provided some constants of the model could to be adapted. Under the supposition of a minimum undercooling, the relation between the average undercooling in front of the isothermal interface (ΔT), the advance interface velocity (V), and the spacing of the fibbers is

$$\Delta T = K_1 V \lambda + \frac{K_2}{\lambda}, \tag{4}$$

where K_1 and K_2 are constants that depend on the system alloy, fundamentally the range of composition between β and η, (ΔC_0), the slopes of the liquidus curve, ($m_{\mathrm{L}}^{\beta,\eta}$), the rate of phase fraction ($f^{\beta,\eta}$), and Gibbs–Thomson coefficient ($\Gamma_{\mathrm{L}}^{\beta,\eta}$) related to each phase [44]. The condition of minimum undercooling supposes that

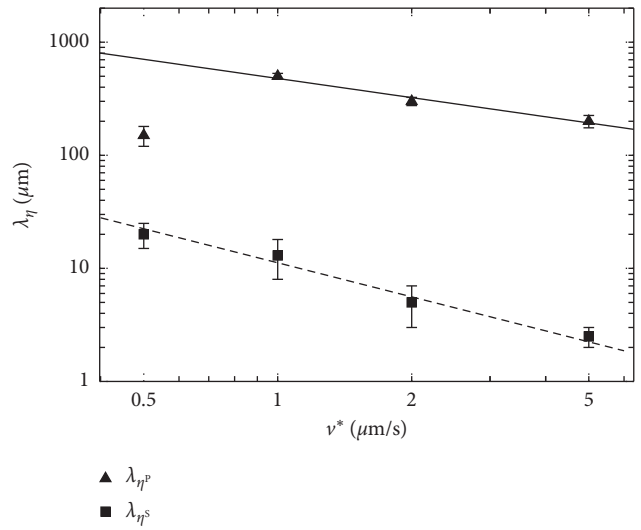

Figure 8: Fiber spacing λ_{η^P} and λ_{η^S} as a function of pulling velocity.

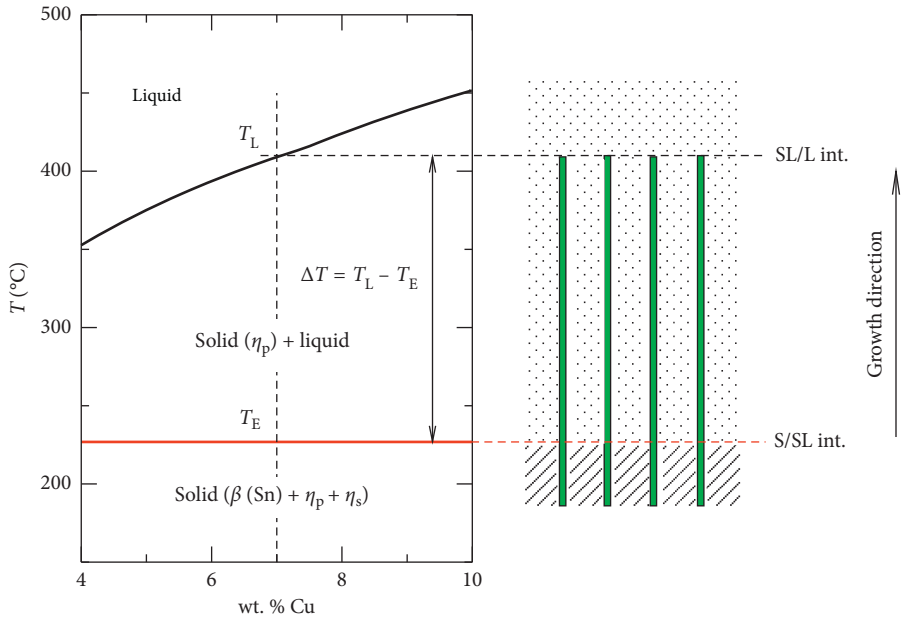

Figure 9: Schematic drawing of the solidification process.

$$\left(\frac{\partial(\Delta T)}{\partial\lambda}\right)_V = 0, \tag{5}$$

which means that

$$\lambda^2 V = K_2/K_1, \tag{6}$$

$$\frac{\Delta T}{V} = 4K_1K_2, \tag{7}$$

$$\lambda\Delta T = 2K_2. \tag{8}$$

Particularly, equation (6) gives a relationship between the spacing and interface velocity:

$$\lambda = K'V^{-1/2}, \tag{9}$$

which in principle could be used in the prediction of the fibber primary phase spacing, as for the eutectic interfibber growth. Following [35], some physical parameters of the Sn-Cu system including K_1 and K_2 can be extracted from the fitted experimental data. In this work, the spacing of the primary fiber λ_{η^P} decreases with the pulling velocity, except the growth corresponding to the smallest velocity, which shows a different tendency. The data can be fitted by the following expression:

$$\lambda_{\eta^P} = 478 \cdot V^{-0.56}\ (\mu\text{m}). \tag{10}$$

In this expression, the constant takes into account the effective thermal gradient in front of the interface. Note that the exponent is close to the predicted one under this formalism. In a similar way, the measured spacing for the secondary or interfibber eutectic can be fitted by the following expression:

$$\lambda_{\eta^S} = 11.2 \cdot V^{-0.96}\,(\mu\text{m}). \tag{11}$$

These two relations are shown together in Figure 8. In this case, as the local growth conditions differ from the conditions found in the front of the growth, both constant and exponent are different.

3.3. Solidification Model. Taking into account the experimental observations previously made including the numerical descriptions of the phase fraction found, it is possible to imagine that the solidification proceeds like it is the schematized in Figure 9. The top of the growth corresponds to η^P fibbers close to the equilibrium condition at the liquidus temperature. In the range in between liquidus and eutectic (solidus) temperatures, this primary phase should persist but is surrounded by the liquid of variable composition from approximately C_0 to C_E, according that solidus temperature is the eutectic T_E.

It is not possible to establish the tip temperature of the growth, to speculate how long from equilibrium is the growth being driven. However, it is not necessarily a big undercooling to let the growth take place, because it is an intermetallic phase. At a first approximation, it can be assumed that the thermal conductivities between involved species solid and liquid are similar; in this case, a simple relation could be postulated to calculate the extension of this zone:

$$\Delta x = \frac{\Delta T_0}{G_L}, \tag{12}$$

where Δx is the length extension of the primary phase into the liquid and ΔT_0 is the solidification range of the alloy at the chemical C_0 composition, which is as follows:

$$\Delta T_0 = T_L(C_0) - T_S(C_0) = T_L(C_0) - T_E, \tag{13}$$

and G_L is the externally applied thermal gradient. In this case, the length is

$$\Delta x \approx 70\,\text{mm}, \tag{14}$$

which corresponds to almost the total length of the samples. Into this zone, the liquid grows with eutectic composition in front of the deeper interface. For this reason, the interfibber solid has the appearance of a eutectic free-growth. However, it is necessary to take into account that the effective thermal gradient in this zone is smaller than G_L externally imposed because of the liquid in thermal contact with the primary phase.

4. Conclusions

The directional solidification of Sn-7 wt.% Cu results in in situ composites of η^P (Cu_6Sn_5) fibbers surrounded by the two-phase eutectic $\beta(Sn) + \eta^S$ (Cu_6Sn_5). Note that the composition of η^P and η^S is the same (Cu_6Sn_5) but have a different origin: the first (η^P) is the primary phase of the growth, whilst the second (η^S) appears during the solidification of the remaining liquid.

The spacing of these phases has a logarithmic dependence with the pulling velocity, similar to a Burden–Hunt growing law, showing different exponents due to the different local solidification conditions of the both interfaces.

Data Availability

All the experimental data used to support the findings of this study are included within the article.

Disclosure

This work was carried out at IFIMAT and CIFICEN.

Conflicts of Interest

The author declares that there are no conflicts of interest.

Acknowledgments

The authors wishes to specially thank the technical staff E. Portalez and O. Toscano. The present work was developed with the economical support of PIP 0627/15 (CONICET) and IFIMAT Institutional Grant (SeCAT-UNCPBA).

References

[1] M. M. Schwartz and S. Aircraft, "ASM Handbook: Welding, Brazing and Soldering," ASM International, Materials Park, OH, USA, 1993.

[2] R. J. K. Wassink, *Soldering in Electronics: A Comprehensive Treatise on Soldering Technology for Surface Mounting and through-Hole Techniques*, Electrochemical Publications Limited, Scotland, 2nd edition, 1989.

[3] R. Strauss, *Surface Mount Technology*, Butterworth-Heinemann, Oxford, UK, 1994.

[4] *Directive 2002/96/EC on Waste Electrical and Electronic Equipment*, European Parliament and the Council, Official Journal of the European Union, vol. 46, pp. 24–38, 2003.

[5] *Directive 2002/95/Ec on the Restriction of the Use of Certain Hazardous Substances in Electrical and Electronic Equipment*, European Parliament and the Council, Official Journal of the European Union, vol. 46, pp. 19–23, 2003.

[6] COST Action MP0602, *Advanced Solder Materials for High Temperature Application (HISOLD)*, European Cooperation in Science and Technology, Brussels, Belgium, 2011.

[7] C. Schmetterer: European Lead Free Soldering Network (projekt), European Cooperation in the Field of Scientific and Technical Research (organizace), COST 531-Lead Free Solders, ELFNET, vol. 2, (K-economy : Knihar, Brno, 2008).

[8] S. W. Yoon, J. R. Soh, H. M. Lee, and B. J. Lee, "Thermodynamics-aided alloy design and evaluation of Pb-free solder, SnBiInZn system," *Acta Materialia*, vol. 45, no. 3, pp. 951–960, 1997.

[9] U. R. Kattner, "Phase diagrams for lead-free solder alloys," *JOM*, vol. 54, no. 12, pp. 45–51, 2002.

[10] N. Moelans, K. C. Hari Kumar, and P. Wollants, "Thermodynamic optimization of the lead-free solder system Bi-In-Sn-

Zn," *Journal of Alloys and Compounds*, vol. 360, no. 1-2, pp. 98–106, 2003.
[11] Z. Moser, W. Gasior, J. Pstrus et al., "Surface tension and density measurements of Sn-Ag-Sb liquid alloys and phase diagram calculations of the Sn-Ag-Sb ternary system," *Materials Transactions*, vol. 45, no. 3, pp. 652–660, 2004.
[12] B. Jönsson and J. Ågren, "Thermodynamic assessment of Sb-Sn system," *Materials Science and Technology*, vol. 2, no. 9, pp. 913–916, 1986.
[13] A. T. Dinsdale, "SGTE data for pure elements," *Calphad*, vol. 15, no. 4, pp. 317–425, 1991.
[14] J. H. Shim, C. S. Oh, B. J. Lee, and D. N. Lee, "Thermodynamic assessment of the Cu-Sn system," *Z Metallkunde*, vol. 87, pp. 205–212, 1996.
[15] K. W. Moon and W. J. Boettinger, "Accurately determining eutectic compositions: the Sn-Ag-Cu ternary eutectic," *JOM*, vol. 56, no. 4, pp. 22–27, 2004.
[16] T. Siewert, S. Liu, D. R. Smith, and J. C. Madeni, *Properties of Lead-Free Solders*, ReleaseNIST and Colorado School of Mines, Golden, Co, USA, 2002.
[17] C. Morando, O. Fornaro, O. Garbellini, and H. Palacio, "Thermal properties of Sn-based solder alloys," *Journal of Materials Science: Materials in Electronics*, vol. 25, no. 8, pp. 3440–3447, 2014.
[18] S. Farina and C. Morando, "Comparative corrosion behaviour of different Sn-based solder alloys," *Journal of Materials Science: Materials in Electronics*, vol. 26, no. 1, pp. 464–471, 2015.
[19] C. Morando, O. Fornaro, O. Garbellini, and H. Palacio, "Fluidity of Sn-based eutectic solder alloys," *Journal of Materials Science: Materials in Electronics*, vol. 26, no. 12, pp. 9478–9483, 2015.
[20] *NPL Lead Free Solder Database-COST Action 531*, Teddington, UK, 2007.
[21] I. Anderson, *Journal of Materials Science: Materials in Electronics*, vol. 18, pp. 55–76, 2007.
[22] W. Liu and N. C. Lee, "The effects of additives to SnAgCu alloys on microstructure and drop impact reliability of solder joints," *JOM*, vol. 59, no. 7, pp. 26–31, 2007.
[23] D. Giuranno, S. Delsante, G. Borzone, and R. Novakovic, "Effects of Sb addition on the properties of Sn-Ag-Cu/(Cu, Ni) solder systems," *Journal of Alloys and Compounds*, vol. 689, pp. 918–930, 2016.
[24] M. J. Rizvi, Y. C. Chan, C. Bailey, H. Lu, M. N. Islam, and B. Y. Wu, "Wetting and reaction of Sn-2.8Ag-0.5Cu-1.0Bi solder with Cu and Ni substrates," *Journal of Electronic Materials*, vol. 34, no. 8, pp. 1115–1122, 2005.
[25] A. A. El-Daly and A. E. Hammad, "Development of high strength Sn-0.7Cu solders with the addition of small amount of Ag and in," *Journal of Alloys and Compounds*, vol. 509, no. 34, pp. 8554–8560, 2011.
[26] D. Li, P. Franke, S. Fürtauer, D. Cupid, and H. Flandorfer, "The Cu-Sn phase diagram part II: new thermodynamic assessment," *Intermetallics*, vol. 34, pp. 148–158, 2013.
[27] S. Amore, E. Ricci, G. Borzone, and R. Novakovic, "Wetting behaviour of lead-free Sn-based alloys on Cu and Ni substrates," *Materials Science and Engineering: A*, vol. 495, no. 1-2, pp. 108–112, 2008.
[28] S. Bader, W. Gust, and H. Hieber, "Rapid formation of intermetallic compounds by interdiffusion in the Cu-Sn and Ni-Sn systems," *Acta Metallurgica et Materialia*, vol. 43, no. 1, pp. 329–337, 1995.
[29] T. Laurila, V. Vuorinen, and J. K. Kivilahti, "Interfacial reactions between lead-free solders and common base materials," *Materials Science and Engineering: R: Reports*, vol. 49, no. 1-2, pp. 1–60, 2005.
[30] G. Zeng, S. D. McDonald, J. J. Read, Q. Gu, and K. Nogita, "Kinetics of the polymorphic phase transformation of Cu6Sn5," *Acta Materialia*, vol. 69, pp. 135–148, 2014.
[31] K. Nogita, C. M. Gourlay, S. D. McDonald, Y. Q. Wu, J. Read, and Q. F. Gu, "Kinetics of the η-η' transformation in Cu6Sn5," *Scripta Materialia*, vol. 65, no. 10, pp. 922–925, 2011.
[32] G. A. O. Feng, N. Hiroshi, and T. Tadashi, *Transactions of JWRI*, vol. 34, pp. 57–61, 2005.
[33] P. Fima, T. Gancarz, J. Pstrus, K. Bukat, and J. Sitek, "Thermophysical properties and wetting behavior on Cu of selected SAC alloys," *Soldering & Surface Mount Technology*, vol. 24, no. 2, pp. 71–76, 2012.
[34] R. Novakovic, T. Lanata, S. Delsante, and G. Borzone, "Interfacial reactions in the Sb-Sn/(Cu, Ni) systems: wetting experiments," *Materials Chemistry and Physics*, vol. 137, no. 2, pp. 458–465, 2012.
[35] E. Çadırlı, U. Böyük, S. Engin et al., "Investigation of the effect of solidification processing parameters on the rod spacings and variation of microhardness with the rod spacing in the Sn-Cu hypereutectic alloy," *Journal of Materials Science: Materials in Electronics*, vol. 21, no. 6, pp. 608–618, 2010.
[36] B. Drevet, D. Camel, M. Dupuy, and J. J. Favier, "Microstructure of the Sn-Cu6Sn5 fibrous eutectic and its modification by segregation," *Acta Materialia*, vol. 44, no. 10, pp. 4071–4084, 1996.
[37] R. N. Grugel and L. N. Brush, "Evaluation of the rodlike cu6sn5 phase in directionally solidified tin-0.9 wt.% copper eutectic alloys," *Materials Characterization*, vol. 38, no. 4-5, pp. 211–216, 1997.
[38] S. McDonald, K. Nogita, J. Read, T. Ventura, and T. Nishimura, "Influence of composition on the morphology of primary Cu6Sn5 in Sn-4Cu alloys," *Journal of Electronic Materials*, vol. 42, no. 2, pp. 256–262, 2013.
[39] O. Fornaro, H. A. Palacio, and H. Biloni, "Segregation substructures in dilute Al-Cu alloys directionally solidified," *Materials Science and Engineering: A*, vol. 417, no. 1-2, pp. 134–142, 2006.
[40] H. Ochoa, O. Fornaro, O. Bustos, and B. Schulz, "Directional solidification of dilute Sn-Pb alloys," *International Journal of Cast Metals Research*, vol. 25, no. 4, pp. 201–206, 2012.
[41] O. Fornaro and C. Morando, "Microstructure development during directional solidification of Sn-Ag-Cu ternary alloys," *International Journal of Cast Metals Research*, vol. 31, no. 2, pp. 118–124, 2018.
[42] M. L. Castro and O. Fornaro, *Acta Microscopica*, vol. 19, pp. 94–99, 2010.
[43] K. A. Jackson and J. D. Hunt, *Transactions of the Metallurgical Society of AIME*, vol. 226, pp. 1129–1142, 1966.
[44] J. A. Dantzig and M. Rappaz, *Solidification*, EPFL Press, Lausanne, Switzerland, 1st edition, 2009.